Analysis of mountain wave 3D wind fields in the Andes derived from high-altitude sailplane flights

Rick Millane[1], Ni Zhang[1], Einar Enevoldson[2] and James Murray[2]
rick.millane@canterbury.ac.nz
[1]*Department of Electrical and Computer Engineering*
University of Canterbury, Christchurch, New Zealand
[2]*NASA Armstrong Flight Research Center, Edwards, CA, USA*

Abstract

Mountain lee waves are of importance in meteorology since they produce drag that affects the general circulation, and can influence windstorms, clear-air turbulence and ozone abundance. Since mountain waves are used routinely by sailplane pilots, data collected during wave flights are potentially useful for studying the structure of mountain waves. We have previously described methods for determining 3D wind velocities in mountain waves from limited sailplane flight data. These methods are applied to data from a high-altitude sailplane flight in the lee of the Andes that reached an altitude of over 15,000 m, well into the stratosphere, allowing a unique kind of in-situ observation of stratospheric mountain waves. The derived wind fields show parts of the wave structure in the troposphere and the stratosphere, and are compared with other observational data. Thus, a minimally instrumented sailplane can provide useful data for mountain wave research.

Introduction

Gravity waves are perturbations in the atmosphere that are driven by gravity and buoyancy [1, 2]. Net forces on a parcel of air can result when the gravitational force on the parcel is not offset by buoyancy forces due to pressure and density differences. The pressure differences associated with gravity/buoyancy forces can produce waves that travel or propagate in the atmosphere, called atmospheric gravity waves. An abrupt change in the pressure or velocity of the air in some region of the atmosphere can act as a source of gravity waves. The way in which gravity waves propagate depends on the source of the waves, but more importantly on the spatial structure (density, temperature, pressure, humidity, etc.) of the atmosphere in the region around the source. The wavelength of gravity waves varies greatly, depending on their nature, and can be up to hundreds of km and more [1, 2].

The gravity waves normally utilized by sailplane pilots are mountain lee waves, whose source is the relatively abrupt change in wind velocity that occurs when air ascends and then descends when flowing over elevated terrain (or mountains) [1, 3]. The waves used for soaring are usually standing, or trapped, waves, that are stationary relative to the terrain. The associated atmospheric pressure perturbation and the vertical wind speed vary approximately sinusoidally with distance downwind from the mountain range. For the case of these trapped waves in the troposphere, the wavelength is typically between 2 km and 20 km [1, 2]. The wave crests may be marked by stationary lenticular clouds where the rising air cools to the dew point. Trapped lee waves exist when the atmospheric conditions are such that the atmosphere forms a horizontal waveguide. This occurs when there is an atmospheric boundary layer, corresponding to a change in the temperature, stability or wind speed profile with altitude, at a particular height. The waves then propagate in the region between the Earth's surface and the boundary layer (or possibly between two boundary layers), and interference effects between different propagating waves lead to a trapped, stationary wave.

Mountain waves useful for soaring are not necessarily completely trapped however, and there may also be some vertical propagation. Although the waves of interest to sailplane pilots are generally in the troposphere, i.e. less that about 10,000 m in altitude (depending on the latitude and the season), they may propagate to higher levels. In some cases they may propagate through the tropopause and high into the stratosphere [4, 5]. Propagation into the stratosphere is favored by a number of conditions, including strong tropospheric mountain waves with some upward propagation, a relatively weak tropopause, and an increasing wind speed in the lower stratosphere which can be assisted by a polar jet from the polar vortex [6].

Gravity waves, both in the troposphere and in the stratosphere, are important because they carry and transfer momentum and

Presented at the XXXII OSTIV Congress, Leszno, Poland, 30 July – 6 August 2014.

energy in the atmosphere, and so affect the general circulation, weather and climate [4, 7]. They can break at points high in the atmosphere where their momentum and energy is dispersed. They can influence the vertical structure of the wind speed and temperature [8]. They can cause fluctuations in wind speeds and strong vertical velocities in the lower atmosphere, and clear air turbulence. They play a role in the vertical transport of aerosols and trace gasses, and can affect ozone concentration [9]. As a result of their importance, gravity waves have been the subject of considerable study and a number of extensive field campaigns [10, 11].

Despite their importance, measurement of the three-dimensional wind field in mountain wave systems is not without difficulty. Radiosondes give information on the horizontal wind speed and direction but only over the radiosonde ascent path. The vertical wind speed can also be estimated from radiosonde flights by correcting for the balloon ascent rate, but this is error-sensitive. Doppler radar is a versatile technique for remote measurement of 3D wind fields, but the equipment required is large and expensive. The most effective method for obtaining data on gravity waves is through the use of specialized research aircraft that are highly instrumented with sophisticated in-situ and remote sensing instrumentation. For example, the Deep Wave Project conducted recently in New Zealand used highly instrumented Gulfstream V and Falcon aircraft, and numerous ground stations, in a very comprehensive field campaign [11].

Mountain waves are a common source of lift used by sailplane pilots, who seek out and effectively explore wave phenomena over extended periods of time and over large geographical areas. Many such flights are conducted each year at various locations around the world. Data from such flights are thus a potentially valuable source of information on the characteristics of mountain waves. There are at least three ways in which one could consider using sailplane flight data to study mountain waves. One would be to use archived flight records. There are potentially many such flight records available, but the information available is limited to the rather scant data that are routinely logged. Furthermore, while some such flights would be of scientific interest, many would not. Second, one could imagine conducting specialized, well instrumented and well documented flights, expressly for scientific research purposes. Although some such flights have been conducted, this is obviously an expensive undertaking. Third, there is an intermediate case where unique flights are undertaken that are reasonably well instrumented, well documented, and for which scientific research may be a secondary factor. Our specific application reported here belongs to this third case.

There have been a number of previous studies of mountain waves using sailplane flight data. Hindman *et al*. [12] describe a quite detailed study using flight data and modelling of a wave flight in the lee of the Catskill Mountains in southern New York State. They used GPS and variometer records. In thermals at lower levels, the horizontal wind speed and direction could be estimated from drift. In wave however, since an air speed record was not available, the horizontal wind speed could not be calculated, and the variometer data could not be corrected to estimate the vertical wind speed. However, by analyzing the maximum and minimum ground speeds, that correspond to downwind and upwind flight segments, respectively, they were able to obtain approximate wind speed estimates in altitude bands. They conducted atmospheric modelling using both 1D linear and high resolution 3D modelling systems. A detailed comparison of the flight data with the modelling results showed that the latter reproduced much of the wave structure experienced during the flight. There have also been some reports of analysis of mountain wave wind fields using sailplane flight data from the Mountain Wave Project [13]. Lindemann *et al*. [14] describe analysis of data from an instrumented motor glider from flights in lee waves of a central region of the Andes. Since their instrumentation included a heading sensor, they were able to extract wind speed and direction information. Using specific flight tracks with a fixed motor power setting, they were able to characterise the wave structure and estimate the vertical momentum transport. Hacker *et al*. [15] describe results from a flight further north in the Andes from Mendoza, also using a motorglider. This flight reached an altitude of 12,000 m, which would have been close to the tropopause. Their instrumentation also included a gust probe and they were able to correlate turbulence (rotor) with wave position and topography. Dummann [16] used data from multiple flights to derive statistical characteristics of lee waves in northern Germany.

For flights for which scientific research is a secondary factor, the instrumentation carried is likely to be similar to that of a standard sailplane set-up. Therefore, the data available in flight records is likely to be quite limited. An important consideration then is what information can be extracted from this limited data, and the development of methods to extract the information. We have considered this problem previously, and in particular the problem of extracting 3D wind fields in mountain waves using sailplane flight data that consists only of a time series of 3D GPS position as well as airspeed [17, 18]. We developed an algorithm to extract the 3D wind field along the flight path and validated it using data from a wave flight in southern California using nearby radiosonde data for the horizontal wind velocity and the overall consistency of the vertical wind speed estimates. This method is briefly reviewed here in Section 2.

The Perlan Project [19] was conceived by Einar Enevoldson in 1992 after seeing evidence of stratospheric mountain waves in LIDAR images. The objectives of the project were to demonstrate that a glider could utilize stratospheric mountain waves to safely fly into the mid stratosphere, to address the associated technical and physiological challenges, and to use such flights as a platform for scientific research [6]. The project developed over subsequent years, with flights conducted using a modified production class glider in California, New Zealand and Argentina. The first phase of the project culminated in 2006 when pilots Enevoldson and Steve Fossett flew to an altitude of approximately 15,000 m (∼50,000 ft) over the Andes in stratospheric

mountain wave. Perlan Project flights thus offer an ideal opportunity to study high-altitude mountain waves. The Perlan Phase 1 project is continued by the Airbus Perlan 2 Project which will use a specially designed sailplane to climb to ∼27 km, high into the stratosphere [19]. This project is well advanced with sailplane construction complete and flights started in 2016.

While there have been a few high-altitude glider flights into the stratosphere, the 2006 Perlan Project flight is the first to provide some useful flight data. It thus provides an ideal data set to which our algorithms can be applied, and used to to study stratospheric mountain waves. Here we present the application of our methods to data from this flight to estimate the 3D wind field and discuss the results.

Methods

We have previously described methods for estimating the 3D vector wind field along the flight path for a sailplane wave flight, using a time series record of only GPS position and airspeed (and pressure and temperature, if available) [17, 18]. We briefly review this method here for the benefit of the reader. The reader is referred to these two references for the details.

It is convenient to estimate the horizontal component of the wind velocity (magnitude and direction) first, and the vertical velocity second. For data consisting of only the ground velocity (derived from the GPS position record) and the air speed, one can derive only a non-unique, one-parameter family of solutions for the horizontal component of the vector wind velocity [17,18]. This is as a result of the lack of aircraft heading data. However, in a wave flight, the wind velocity can be considered to be quasi-stationary in space and time. If ground velocity data are available for a variety of (unknown) headings within spatio-temporal regions that are smaller than the characteristic scale of the wind velocity field, then the one-parameter ambiguity can be resolved [17]. This is the basis of our approach, and the characteristic scales are typically of the order of 2 km horizontally, 100 m vertically, and 10 min temporally.

Our algorithm for estimating the horizontal wind velocity involves the following steps. (1) Calculate the horizontal ground velocity from the GPS position data. (2) Convert the indicated air speed (IAS) to true air speed (TAS) (using either pressure and/or temperature recording, or using a standard atmosphere and the GPS altitude). (3) Divide the flight path into spatio-temporal regions. Within each region, (4) use pairs of ground velocity and air speed data to calculate pairs of horizontal wind velocity estimates, and (5) use a clustering analysis to determine a unique wind velocity estimate and the associated errors. Repeating steps (4) and (5) for each region gives horizontal wind vector estimates and associated precision at positions along the flight path.

Estimation of the vertical wind speed estimates involves the following steps. (1) Calculate the vertical ground speed from the GPS altitude data. (2) Calculate the sailplane sink rate using the IAS and the flight polar (and scaled by the TAS/IAS ratio). (3) Calculate the sailplane acceleration from the TAS and use this to calculate the vertical speed component due to potential-kinetic energy exchange. (4) Use these three vertical velocities to calculate the vertical wind speed. (5) From the flight path and the horizontal wind velocity estimate, calculate the flight path relative to the air, and with the TAS calculate the sailplane bank, and exclude any vertical wind speed estimates (considered to be potentially unreliable) that correspond to excessive bank. This gives the vertical wind speed estimates along the flight path.

The 3D (horizontal and vertical) wind velocity estimates are then displayed and analyzed in various ways as described in the next section.

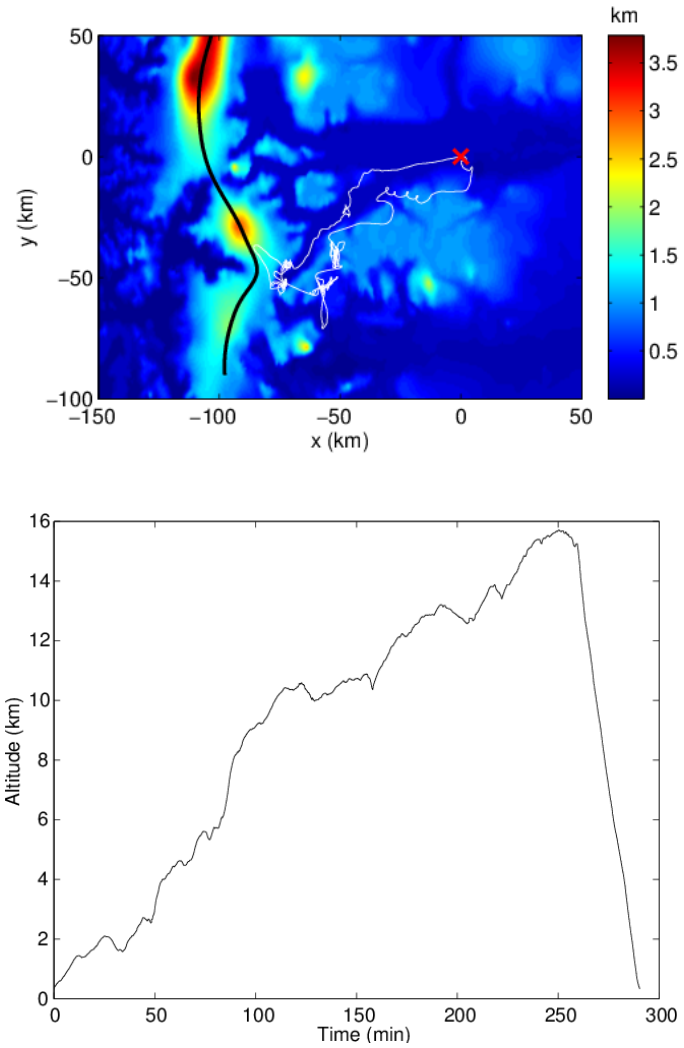

Fig. 1: Flight path and topography (altitude scale shown in the color bar) (top). The red cross denotes the take-off point at EI Calafate, the thick black line denotes the estimated ridge line, and the white line denotes the flight path. Flight altitude versus time (bottom).

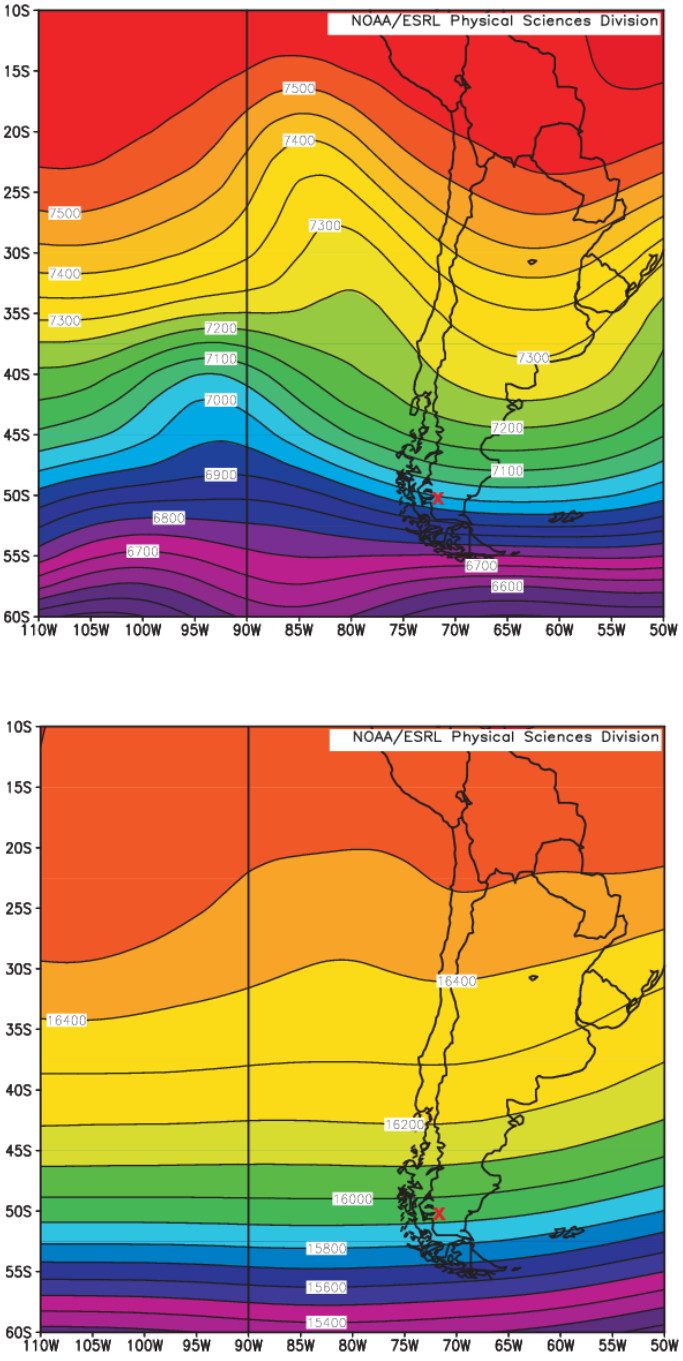

Fig. 2: Geopotential height (m), composite mean from 1200Z to 1800Z, for the Southern Andes at 400 mb (top) and 100 mb (bottom) extracted from the Global Reanalysis [20]. The take off position for the flight is marked by the red cross.

Results

Results are presented for Perlan Project flight No. 66 which took place in Argentina in the 2006 Southern Hemisphere winter. The pilots were Einar Enevoldson and Steve Fossett. The sailplane was a two-seat production Glaser-Dirks DG-505M (DG Flugzeugbau GmbH, Bruchsal, Germany) specially equipped for high altitude flight and flown at an all up weight of 805 kg (wingspan 20 m and wing loading 45 kg/m^2). The maximum altitude possible with the modified configuration was calculated as 20,000 m (62,000 ft). To estimate the effects of the modifications to the DG-505M on the flight polar, comparison flights were made with another standard sailplane, the sink rates compared, and minor modifications made to the 45 kg/m^2 wing loading DG-505M polar from the flight manual [17]. The sink rate varies between approximately 0.5 and 1.3 m/s at 25 and 40 m/s IAS, respectively.

In addition to the usual instruments, the sailplane was equipped with a modified Volkslogger GPS positioning system and pressure transducer (Garrecht Avionik GmbH, Bingen, Germany), a Borgelt B-50 variometer system (Borgelt Instruments, Toowoomba, Australia), and a Platinum RTD (resistance temperature detector) outside air temperature probe. GPS fixes were obtained at 1 second intervals from the Volkslogger and pressure recordings made at 8 second intervals. Airspeed (from the Borgelt B-50) and temperature measurements were made at approximately 2.5 second intervals. All data were merged into a serial data stream and recorded on a custom data logger. All data (except GPS fixes) were linearly interpolated onto the one-second GPS time-stamps post flight. The data consisting of GPS position, indicated airspeed, pressure and temperature were used for the analysis.

The sailplane was launched from the airport Aeropuerto El Calafate in Patagonia, Argentina (50.3S 72.1W, altitude 207 m) at 1410Z on 29 August 2006 (1110 local time), flew along Lake Argentino, south to the Cervo Pietronrlli mountain range, then

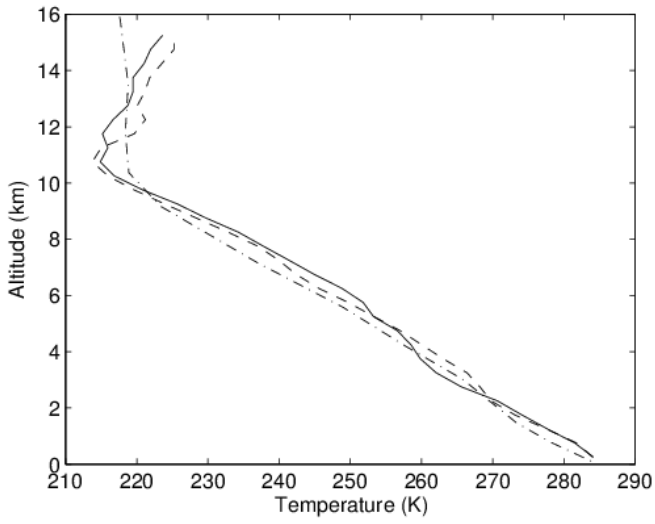

Fig. 3: Temperature versus altitude measured along the ascending (solid line) and descending (dashed line) flight path. Temperature extracted from the reanalysis is shown by the dot-dashed line.

north along the ridges, and finally back to the airport. The duration of the flight was 4.8 hours. The flight path and the topography are shown in Figure 1. The flight proceeds approximately anticlockwise around the path shown. The flight altitude versus time is also shown in Figure 1. The flight reached a maximum altitude of 15,447 m (50,671 ft), which was a new absolute altitude world record for gliders. The topography is dominated by the eastern ridge of the Southern Andes mountain range, running North-South, to the west of the flight path. The center line of this ridge is taken as a topographical reference which is referred to as the "ridge-line." Points at maximum altitude along this ridge were located manually and the ridge-line determined by spline interpolation. The estimated ridge-line is shown as the thick black line in Figure 1 and the launch position is marked by the cross. The geopotential height at 400 mb and 100 mb (approximately 7,000 m and 16,000 m, in the troposphere and stratosphere, respectively) for the region and time of the flight was extracted from the NCEP/NCAR Global Reanalysis [20] and is shown in Figure 2. The high pressure region to the North gives a westerly air flow.

The temperature data recorded for the ascending and descending portions of the flight were collected into altitude bins 200 m thick and averaged, and are shown versus altitude in Figure 3. There is a clear temperature inversion at approximately 11 km corresponding to the tropopause. The flight therefore ascended 4.5 km into the stratosphere. Fitting two line segments to the temperature data gives lapse rates of -6.0 K/km in the troposphere, and +2.2 K/km in the stratosphere. The temperature at the launch site extracted from the reanalysis is also shown in Figure 3 and shows good agreement with the measured data. The lapse rates from the reanalysis are approximately -6.8 K/km below 10 km and zero above 10 km, in fairly good agreement with the data.

The flight data were processed as described previously [17, 18]. For calculation of the horizontal wind velocity, the flight path was partitioned into 211 regions, 84 of which gave good horizontal wind velocity estimates. The wind velocity estimates along the flight path are shown in Figure 4. Circling flight is evident near the North-East region of the flight path and the derived wind direction is consistent with the drift seen during the circling flight. As described previously, with only GPS position and airspeed, the wind velocity can be estimated reliably only where the heading is changing. The straight flight segments therefore do not give wind velocity estimates as shown. Clusters of wind velocity estimates are evident in the circling and curved segments of the flight path. The wind speed and direction estimates were collected into altitude bins 500 m thick and averaged for the whole flight, and are shown versus altitude in Figure 5.

The wind direction is relatively constant over the entire altitude range at $280 \pm 15^\circ$, and the small variation indicates the quality of the wind velocity estimates. The small westerly shift in the wind direction at altitude is consistent with the small rotation of the contours seen in Figure 2. The wind speed increases up to 40 m/s at 4,000 m, decreases to 30 m/s at about 8,000 m, and increases to about 45 m/s at the maximum altitude of 15,000 m. The wind speed and direction extracted from the reanalysis are also shown in Figure 5. Inspection of the figure shows that the measured wind direction is consistent with that from the reanalysis with an rms difference of 8°. Although the overall measured wind speed is similar to that of the reanalysis, there are some quite large differences, up to about 10 m/s, along the altitude profile. Whereas the data show a reduced wind speed in the mid troposphere, the reanalysis indicates an increased wind speed. The data then show an increasing wind speed up to the lower stratosphere, whereas the reanalysis shows a decreasing wind speed. The reason for these differences is not clear. However, the flight data give local wind speed estimates at positions along the flight path that vary horizontally by up to 100 km. The reanalysis wind speeds, on the other hand, are averages within horizontal resolution cells that are about 100 km across. Therefore, one cannot necessarily make direct comparisons between these two kinds of wind speed estimates.

The vertical wind speed along the flight path was calculated as described previously [17, 18] and is displayed in Figure 6. In order to show the vertical wind speed as a function of altitude and position relative to the topography, it is plotted in Figure 6 versus altitude and distance downwind from the ridge-line. The flight path is projected onto this coordinate system and the vertical wind speed is coded by color. In this figure, the flight begins at the lower center and proceeds up, towards and then away from the ridge-line, to the maximum altitude. The descent phase is to the right in the figure. Inspection of the figure shows clear regions of large vertical wind velocities (upwards), in the tro-

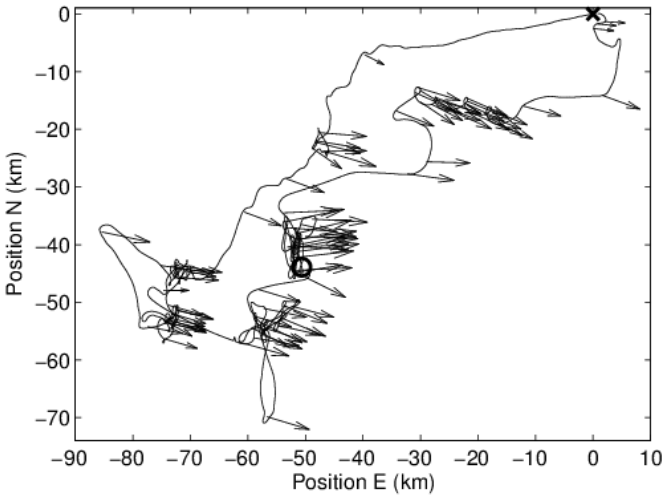

Fig. 4: Wind velocity vectors calculated from the flight data shown by arrows at the corresponding positions along the flight path. The launch position is shown by the x and the flight path is approximately anticlockwise. The position of maximum altitude of the flight is marked by the circle.

posphere, through the tropopause, and in the stratosphere. This allows the positions of the leading (upwind) edges of the wave to be located, and the main such upwind wave lines are shown in a horizontal Cartesian coordinate system oriented parallel to the wind direction in Figure 6. Lining up of the wave rising edges parallel to the ridge-line and their fairly regular spacings in the down-wind direction are evident.

A good picture of the local spatial structure of the vertical wind speed in the wave derived from the flight data requires flight segments that are either upwind or downwind over distances of several wavelengths. Two such downwind segments are marked by the ellipses in Figure 6. The first segment is in the troposphere at an altitude of about 6,000 m and the second segment is in the stratosphere at an altitude of about 15,000 m. The vertical wind speeds in these two segments are plotted versus distance downwind from the ridge-line in Figure 7. Sinusoids were fitted to these vertical wind speeds as shown. About two wavelengths are seen, and the sinusoid in the troposphere has an amplitude of 4 m/s and a wavelength of 9 km, and that in the stratosphere an amplitude of 4 m/s and a wavelength of 22 km.

A GOES-12 visible satellite picture corresponding to the flight location and time is shown in Figure 8 [21]. The picture is at 1745Z, which is 3.5 hours into the flight and 40 minutes prior to the time of maximum altitude. The picture shows a solid cloud sheet to the west of the ridge-line, and some regularly spaced cloud features to the East, aligned approximately parallel to the ridge-line. The spacing between the leading edges of the

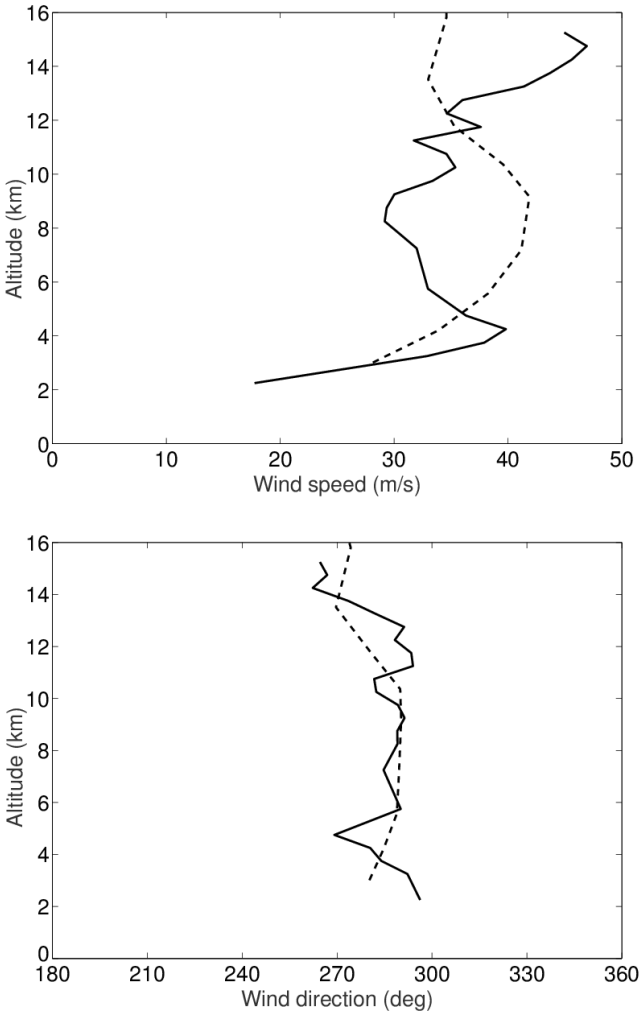

Fig. 5: Horizontal wind speed (top) and direction (bottom) versus altitude calculated from the flight data (solid lines). The horizontal wind speed and direction extracted from the reanalysis are shown by the dashed lines.

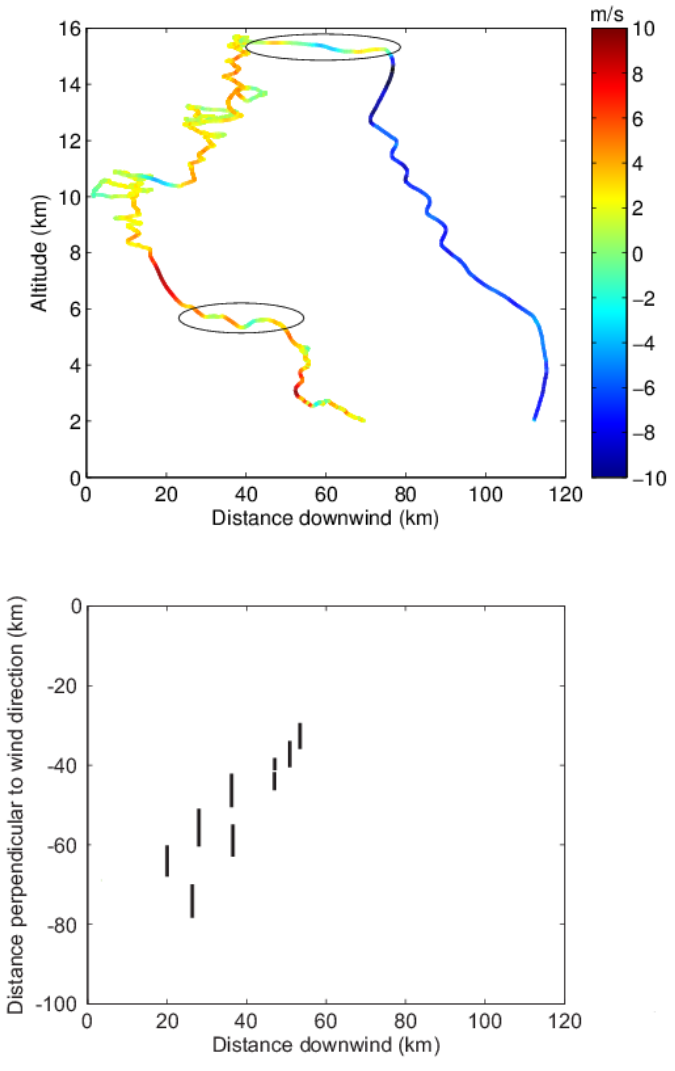

Fig. 6: Vertical wind speed (colour coded as indicated) calculated from the flight data versus altitude and distance downwind from the ridge-line (top). Estimated positions of the leading (rising) edges of the wave in the horizontal plane (bottom).

clouds in the region of the maximum flight altitude is approximately 25 km. The regular cloud pattern suggests a relationship to wave activity, but the spacing is difficult to interpret without cloud top height data. The cloud spacing, however, is consistent with the wavelength of 22 km in the stratosphere derived from the flight data.

The characteristics of mountain waves can be described with the help of the Scorer parameter [22], ℓ, given by

$$\ell = \frac{N}{U} = \frac{1}{U}\sqrt{\frac{g}{T}\left(\Gamma - \Gamma_a\right)}\,, \tag{1}$$

where N is the buoyancy (Brunt-Väisälä) frequency, U is the wind speed, g is the acceleration due to gravity, T is the temperature, Γ is the (environmental) lapse rate, and Γ_a is the adiabatic lapse rate. Note that here we use the convention that Γ is negative for a temperature that decreases with increasing altitude. The Scorer parameter depends on altitude as a result of the altitude-dependence of the quantities on the right-hand-side of Eq. (1). In practice, the structure of mountain waves is a complex function of the vertical structure of the atmosphere, and also the shape of the forcing topography, and cannot be described by a single parameter, although the Scorer parameter can give some insight. The natural wavelength for stationary gravity waves, λ_n, is

$$\lambda_n = \frac{2\pi}{\ell}\,. \tag{2}$$

The most favorable conditions for the formation of trapped, or stationary, gravity waves, or mountain waves, is when the Scorer parameter decreases with altitude [3, 22]. The natural wavelength therefore varies with altitude, but for trapped waves a single wavelength is selected, typically within the range of natural wavelengths within the layer. For vertically propagating (untrapped) waves, the natural wavelength given by Eq. (2) represents a minimum value, and the actual wavelength can be much larger than this value [2, 3].

The Scorer parameter was calculated using Eq. (1) and the wind speed and temperature versus altitude derived from the flight data, and is shown versus altitude in Figure 9. It decreases up to an altitude of 4,000 m, shows a small increase between 4,000 and 9,000 m, increases abruptly at the tropopause, and decreases with increasing altitude in the stratosphere. The increasing Scorer parameter between 4,000 and 9,000 m is somewhat unexpected in the presence of mountain waves, and results from the decreasing wind speed in this altitude band that is derived from the flight data as described above. However, as described above, there is some difficulty with making average interpretations using derived wind speeds that are over a wide range of horizontal positions. The larger value in the stratosphere is due

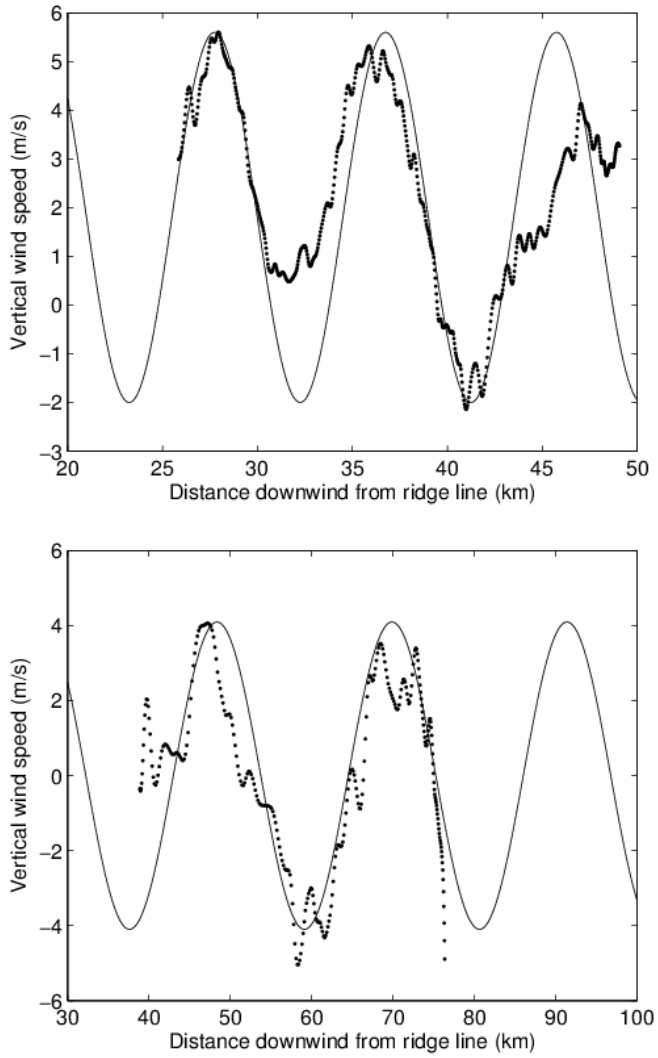

Fig. 7: Vertical wind speed versus distance downwind from the ridge-line calculated from the flight data, and fitted sinusoids, for flight segments in the troposphere (top) and stratosphere (bottom), as described in the text.

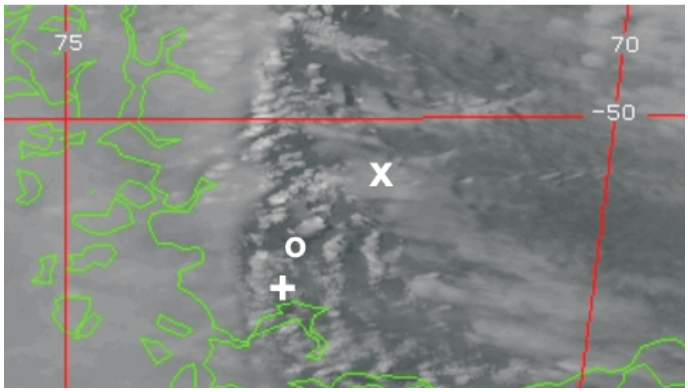

Fig. 8: Geostationary satellite GOES-12 picture, band 1 (visible), of Southern Argentina in the region of the flight at 1745Z [21]. The takeoff position is marked by the x, the most Southern position of the flight by the +, and the position of the highest altitude of the flight by the circle.

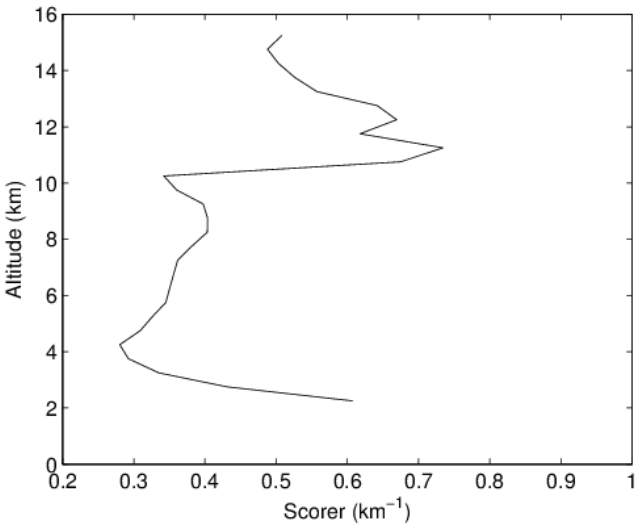

Fig. 9: Scorer parameter versus altitude.

to the positive lapse rate, and the subsequent decrease with altitude is a result of the increasing wind speed. The decreasing Scorer parameter in the lower troposphere may be associated with the development of trapped waves, and the small increase in the mid and upper troposphere, which is not conducive to trapping, may assist with some vertical propagation into the stratosphere. The natural wavelength in the troposphere calculated using Eq. (2) varies between about 10 and 20 km, compared to the observed wavelength of 9 km at 6,000 m. In the stratosphere, the natural wavelength from Eq. (2) varies between about 9 and 12 km. Gravity waves in the stratosphere are likely to be vertically propagating, with wavelengths larger than the natural wavelength, which is consistent with the observed wavelength of 22 km.

Summary

Gravity waves are of fundamental importance in meteorology and climate science. They can be probed using various forms of remote sensing, and by in-situ methods using dedicated flights with specialized research aircraft. Sailplane flights in mountain waves offer a unique measurement platform as a result of their propensity to explore mountain wave systems, and their simple and well-characterized aerodynamics. Routine sailplane flights could be considered as "sensors of opportunity," and more specialized flights could be dedicated to mountain wave research. The minimal instrumentation routinely carried by sailplanes is potentially problematic, but with suitable algorithms, useful information can be obtained from the available data.

Analysis of flight data from a minimally-instrumented, high-altitude flight in the lee waves of the Andes shows the potential of this approach, and provides unique observations of stratospheric mountain waves. Horizontal wind fields along the flight path are calculated from the flight data and the wind directions obtained agree well with reanalysis calculations. There are some differences to reanalysis wind speeds, which may be due to the differing resolutions of the two estimates. Calculation of vertical wind speeds from the flight data shows the positions and strengths of upwind edges of the wave throughout the troposphere, tropopause, and stratosphere. Derived wavelengths are overall consistent with a simple model based on the Scorer parameter. The results presented show the potential for the use of sailplane flight data for mountain wave research.

References

[1] Scorer, R. S., *Dynamics of Meteorology and Climate.*, Academic Press, San Diego, CA, USA, 1997.

[2] Nappo, C., *Introduction to Atmospheric Gravity Waves.*, Academic Press, San Diego, CA, USA, 2012.

[3] Etling, D., *Atmospheric Gravity Waves and Soaring Flight.*, Published by the author, Hannover, Germany, 2014.

[4] Eckermann, S. D. and Preusse, P., "Global measurements of stratospheric mountain waves from space." *Science*, Vol. 286, No. 5444, 1999, pp. 1534–1537.

[5] Smith, R. B., Woods, B. K., Jensen, J., Cooper, W. A., Doyle, J. D., Jiang, Q., and Grubisic, V., "Mountain waves entering the stratosphere." *J. Atmos. Sci.*, Vol. 65, 2008, pp. 2543–2562.

[6] Teets, E. H. and Carter, E. J., "Atmospheric conditions of stratospheric mountain waves: Soaring the Perlan aircraft to 30 km." *Proc. 10th Conf. Aviation, Range Aerospace Meteor.*, American Meteorological Society, 2002, pp. 195–198.

[7] Holton, J. R., "The influence of gravity wave breaking on the general circulation of the middle atmosphere." *J. Atmos. Sci.*, Vol. 40, 1983, pp. 186–201.

[8] Sato, K., "Vertical wind disturbances in the troposphere and lower stratosphere observed by the MU radar." *J. Atmos. Sci.*, Vol. 47, 1990, pp. 2803–2817.

[9] Bird, J. C., Pal, S. R., Carswell, A. I., Donovan, D. P., Manney, G. L., Harris, J. M., and Uchino, O., "Observations of ozone structure in the Arctic polar vortex." *J. Geophys. Res.*, Vol. 102, No. D9, 1997, pp. 10785–10800.

[10] Smith, R. B., Doyle, J. D., Jiang, Q., and Smith, S. A., "Alpine gravity waves: Lessons from MAP regarding mountain wave generation and breaking." *Quart. J. Roy. Meteor. Sci*, Vol. 133, No. 625, 2007, pp. 917–936.

[11] www.eol.ucar.edu/field_projects/deepwave

[12] Hindman, E. E., McAnelly, R. L., Cotton, W. R., Pattist, T., and Worthington, R. M., "An unusually high summertime flight." *Technical Soaring*, Vol. 28, No. 4, 2004, pp. 7–23.

[13] www.mountain-wave-project.com

[14] Lindemann, C., Heise, R., and Herold, W., "Lee waves in the Andes region, mountain wave project (MWP) of OSTIV." *Technical Soaring*, Vol. 32, No. 3, 2008, pp. 93–96.

[15] Hacker, J. M., Heise, R., Ohlmann, K., Herold, W. D., Gaissmaier, R. W., Hub, R., and Alvarez, E., "Measuring mountain waves and turbulence at up to 12 km altitude over the Andes in South America in an instrumented motorised glider." *Proc. 14th National AMOS Conference*, Australian Meteorological and Oceanographic Society (AMOS), 2007.

[16] Dummann, J., "A report on glider pilot activities to document lee wave events in northern Germany and their aims." *Technical Soaring*, Vol. 33, No. 4, 2009, pp. 109–116.

[17] Millane, R. P., Stirling, G. D., Brown, R. G., Zhang, N., Lo, V. L., Enevoldson, E., and Murray, J. E., "Estimating wind velocities in mountain waves using sailplane flight data." *J. Atmos. Ocean. Technol.*, Vol. 27, 2010, pp. 147–158.

[18] Zhang, N., Millane, R. P., Enevoldson, E., and Murray, J. E., "Measuring 3D wind fields in mountain waves using sailplane flight data." *Technical Soaring*, Vol. 36, No. 3, 2012, pp. 57–66.

[19] www.perlanproject.org

[20] NCEP/NCAR Reanalysis Datasets, Physical Sciences Division, Earth Systems Research Laboratory, NOAA. Available at www.esrl.noaa.gov/psd.

[21] Environmental Data from Geostationary Satellites, Comprehensive Large Array-data Stewardship System, NOAA. Available at www.nsof.class.noaa.gov.

[22] Scorer, R. S., "Theory of waves in the lee of mountains." *Quart. J. Roy. Meteor. Soc.*, Vol. 75, No. 323, 1949, pp. 41–56.